Bosshardt Dieter D (Orcid ID: 0000-0002-2132-6363)
Roccuzzo Mario (Orcid ID: 0000-0002-2135-6503)

Benchmark performance of anodized vs. sandblasted implant surfaces in an acute dehiscence type defect animal model

Short title: Gradient anodized vs. moderately rough implants in dehiscence type defects

Shakeel Shahdad[1,2], Dieter Bosshardt[3], Mital Patel[1,2], Nahal Razaghi[1], Anuya Patankar[1], Mario Roccuzzo[4,5,6]

1 Barts Health NHS Trust, The Royal London Dental Hospital, London, UK.

2 Barts and The London School of Medicine and Dentistry, Queen Mary University of London, London, UK.

3 Department of Periodontology, University of Bern, Bern, Switzerland

4 Private practice, Torino, Italy.

5 Department of Maxillo-facial Surgery, University of Torino, Torino, Italy.

6 Department of Periodontics and Oral Medicine, University of Michigan, Ann Arbor, Michigan, USA

Corresponding author: Shakeel Shahdad, Department of restorative Dentistry, The Royal London Dental Hospital, Turner Street, E1 1DE, London, UK. Email: s.shahdad@qmul.ac.uk

Keywords: osseointegration, crestal bone formation, implant surface, implant geometry, dehiscence type defects

Abstract word count: 295 words, Total word count (end of abstract to the beginning of acknowledgment): 6031 words, 6 figures, 1 table. 31 references.

Acknowledgment

The author would like to thank Leticia Grize for the statistical analysis and Novonexile AG (Switzerland) for writing assistance and editorial support in preparing the manuscript.

Conflict-of-interest statement

The present study was funded by a grant from Intitut Straumann AG. SS and MR receive speaker honorariums for educational courses from Institut Straumann AG. DB, MP, NR and AP declare no conflict of interest.

Author contributions

SS: Conceptualization, Data curation, Investigation, Methodology, Project Administration Writing – original draft; DB: Formal Analysis, Methodology, Resources, Validation, Writing – review & editing; MP & NR: Data curation, investigation, resources, validation, Writing – review & editing; MR: Funding acquisition, methodology, resources, supervision, validation, writing – review & editing

This article has been accepted for publication and undergone full peer review but has not been through the copyediting, typesetting, pagination and proofreading process which may lead to differences between this version and the Version of Record. Please cite this article as doi: 10.1111/clr.13996

1 Abstract

Objectives

Crestal bone formation represents a crucial aspect of the esthetic and biological success of dental implants. This controlled preclinical study analyzed the effect of implant surface and implant geometry on de novo crestal bone formation and osseointegration.

Materials and methods

Histological and histomorphometrical analysis was performed to compare three implant groups, i.e., (1) a novel, commercially available, gradient anodized implant, (2) a custom made geometric replica of implant "1", displaying a superhydrophilic micro-rough large-grit sandblasted and acid-etched surface and (3) a commercially available implant, having the same surface as "2" but a different implant geometry. The study applied a standardized buccal acute-type dehiscence model in minipigs with observation periods of 2 and 8 weeks of healing.

Results

The amount of newly formed crestal bone (BATA) around control group (2) and (3) was significantly increased when compared to the test group (1) at the 8-weeks healing time point. Similar results were obtained for all parameters related to osseointegration and direct bone apposition, to the implant surface (dBIC, VBC, and fBIC), demonstrating superior osseointegration of the moderately rough, compared to the gradient anodized functionalization. After 2 weeks, the osseointegration (nBIC) was found to be influenced by implant geometry with group (3) outperforming group (1) and (2) on this parameter. At 8 weeks, nBIC was significantly higher for group (2) and (3) compared to (1).

Conclusions

The extent (BATA) of de novo crestal bone formation in the acute-type dehiscence defects was primarily influenced by implant surface characteristics and their ability to promote osseointegration and direct bone apposition.

Osseointegration (nBIC) of the apical part was found to be influenced by a combination of surface characteristics and implant geometry. For early healing, implant geometry may have a more pronounced effect on facilitating osseointegration, relative to the specific surface characteristics.

2 Introduction

Osseointegrated dental implants have become a well-established modality for replacing missing teeth (Albrektsson et al. 1986). Technological improvements and increased patient demands have recently triggered a shift towards shorter and even immediate implant procedures (Buser et al. 2017). Likewise, the clinical outcome of dental implant procedures is not evaluated purely on functional requirements but, increasingly, in terms of biological and esthetic considerations. (Choquet et al. 2001; Misch et al. 2008; Huang et al. 2021).

The anatomic parameters influencing immediate implant placement are well understood (Kan et al. 2011). Optimized osteotomy preparation techniques, geometrical implant designs and surface modifications have been introduced to allow high primary and secondary stability (Puleo 1999; Javed et al. 2013; Wilson et al. 2016).

Following implant placement and restoration, the crestal hard and soft tissues are subjected to ongoing changes (Albrektsson et al. 1986; Atsuta et al. 2016). Often a gradual recession of the soft tissues around the implant, in conjunction with the resorption of supportive underlying crestal bone, can be observed (Atsuta et al. 2016). Consequently, high peri-implant crestal bone levels and a tight coronal soft tissue barrier have been proposed as critical for the long-term esthetic success of implant supported restorations (Laurell & Lundgren 2011; Atsuta et al. 2016).

Various implant designs and placement strategies have been introduced to achieve and maintain high crestal bone levels (Laurell & Lundgren 2011; Valles et al. 2018). Changes in the surface roughness and hydrophilicity of the coronal aspect of the implant have, e.g., been shown to effectively promote coronal bone growth and limit marginal bone loss, respectively (Schwarz et al. 2007; Hermann et al. 2011; De Bruyn et al. 2017). Subcrestally placed platform switched implants have also proven effective in limiting crestal bone loss (Valles et al. 2018). Recently, based on the hypothesis that marginal bone loss around rough implant surfaces might be higher, compared to machined or moderately rough implant surfaces (De Bruyn et al. 2017; Milleret et al. 2019; Susin et al. 2019), a new implant concept has been developed. Specifically, this implant concept is based on a novel gradient anodized (NGA) surface with a 2 mm zone, at the coronal implant collar, displaying minimal roughness (Milleret et al. 2019). Some controversy remains, however, to the effectiveness of this approach. Earlier clinical pilot studies, investigating subcrestal placement of implants with a smooth (either polished or machined) to rough transition, indicate that such configurations may not yield desirable results (Hämmerle et al. 1996; Hartman & Cochran 2004)

Given the importance of high crestal bone levels for the biologic and esthetic success of dental implants, the present study aimed to test the performance of NGA implants in comparison to implants modified with the established superhydrophilic moderately rough sandblasted acid-etched surface. The relative performance was investigated using a standardized buccal acute-type dehiscence model in minipigs, assessing crestal bone formation and osseointegration (Rupp et al. 2006; Bosshardt et al. 2017). Considering the potential influence of implant design on the osseointegration process, the study was designed to allow for distinguishing the relative contributions from surface characteristics and implant geometry.

3 Materials and methods

3.1 Study design

This controlled preclinical study aimed to investigate the influence of surface characteristics and implant geometry on their potential to promote crestal bone formation and osseointegration. The tested implants are schematically depicted in Figure 1A. In the following description, the three implant groups are designated by their group number followed by their role in the study. Moreover, information on the implant type, surface functionalization, base material, implant dimensions and manufacturer is listed in parenthesis, for each implant group. The impact of surface characteristics was investigated by comparing (**1**, Test group) NGA functionalized, commercially available, implants (NobelActive, TiUltra NP, commercially pure Titanium, 3.5 x 8.5 mm, Nobel Biocare AG, Switzerland) with (**2**, Surface functionalization control group) custom made replicas of the NGA implant geometry, modified with the SLActive surface (Replica of NobelActive, SLActive, Roxolid, 3.5 x 8.5 mm, Institut Straumann AG, Switzerland). Additionally, the potential influence of implant geometry was investigated by including (**3,** Implant geometry control group) a commercially available BLX implant (BLX, SLActive, Roxolid, 3.5 x 8 mm, Institut Straumann AG, Switzerland). All control implants were manufactured according to standard procedures for commercial implants (Institut Straumann AG, Switzerland).

De-novo crestal bone formation was analyzed histologically and histomorphometrically using a standardized acute type buccal dehiscence model after 2 and 8 weeks of healing. This model has previously proven effective for comparing implant surface modifications and was adopted in the mandible of minipigs for the current study (Schwarz et al. 2007, 2008).

A total of 15 Göttingen minipigs™, i.e., 7 animals for the 2 weeks time point and eight animals for the 8 weeks time point was included in the study. Study groups were compared by intra-animal comparison using one type of implant (group) per animal, for each study group. Implant positions were altered between animals by a rotation scheme, to ensure that each implant was represented the maximum number of times at each anatomical position (left/right and mesial/distal) across the animals per healing period. Furthermore, due to the primary endpoint targeting the surface comparison and the geometry only as a secondary endpoint, care was taken to ensure Groups 1 and 2 were always placed on contralateral sides from one another. Each study group at the different healing periods had a n=6 for the 2 weeks healing and a n=8 for the 8 weeks healing. To reduce the number of animals used for research, each animal received three additional implant groups, i.e., a total of 6 implants per animal that were part of a different study.

This study was conducted at the Biomedical Department of Lunds University (Lund, Sweden) and approved by the local Ethics Committee of the University (M-192-14) following the proper institutional and national guidelines for the care and use of the animals in the study. This study adhered to the ARRIVE 2.0 Guidelines and was designed by considering the 3R principle for animal research (Percie du Sert et al., 2020).

3.2 Replication of NGA test implants and characterization of moderately rough control implants

Implants of group **1** and **2** were scanned using microCT (Zeiss Metronom 1500 G3, Zeiss, Germany) with a votage of 15 kV, a current of 100 µA and an averaging time of 2000 ms from a flat part position and a resolution of 0.015mm. The raw data files were converted into CADCAM format using the program Design X (v2020.0, 3D Systems, Germany). Implant blanks were milled of TiZr and subsequently surface-modified as described above according to standard procedures (Institut Straumann AG, Switzerland).

Implants of group **1** and **2** were compared in terms of microCT scan overlays (VGStudio Max, v3.4.5, Volume Graphics, Germany) (Figure 1), scanning electron microscopy (Figure 2, surface roughness measurements, and dynamic contact angle measurements (DCA) (Table 1).

Surface analyses were carried out as previously described (Pippenger et al. 2019). In brief, advancing contact angles were measured by the dynamic Wilhelmy method on a KRÜSS K100 tensiometer (Krüss GmbH, Germany) in deionized water. Surface roughness was assessed using

a µsurf explorer confocal microscope and µsoftAnalysisXT software (NanoFocus AG, Germany) at 20x magnification. Surface parameters were evaluated on 798 x 798 μm^2 using a Gaussian wavelength cutoff of 50 x 50 μm^2. Surface roughness was quantified in S_a values, as defined by the average height deviation from the mean plane.

Surface morphology was evaluated using a Zeiss Supra 55 SEM (Carl Zeiss AG, Germany) equipped with an Everhart-Thornley secondary electron detector at high and low acceleration voltages of 15kV and 5kV, respectively. Surface characteristics were determined as triplicates and are reported as mean values.

3.3 Animals

15 female Göttingen Minipigs™ (Ellegaard, Denmark) of age between 20-24 months at the time of surgery and an average body weight of 40 kg were included in the study. The animals were housed in standard boxes in groups of three. Animals were adapted to experimental conditions by starting animal housing one week before intervention. Animals were fed a standard soft food diet (Special Diet Services (SDS), Witham, UK #801586). Animals were fasted overnight before surgery, to prevent vomiting.

3.4 Surgical procedure

All surgical procedures were performed under general anesthesia using a combination of dexmedetomidine (25-35 µg/kg i.m., Dexdomitor; Orion Pharma Animal Health) and tiletamine-zolazepam (50-70 mg/kg i.m., Zoletil 100 Vet, Virbac) injected intramuscularly and maintained with intravenous infusion after induction with propofol (PropoVet multidose, Orion Pharma Animal Health) and fentanyl (Fentanyl B. Braun). Carprofen (4mg/kg, s.i.d., i.m., Rimadyl vet., Orion Pharma Animal Health) was given as a preemptive dose and postsurgically up to 4 days together with buprenorphine (0,03mg/kg, i.m., Vetergesic vet, Orion Pharma Animal Health). To reduce the dosage of the systemic anesthetic, bleeding during surgery, and to alleviate post-surgical pain, local anesthesia was provided intraoperatively by infiltrative injection of 1.8 ml of Xylocaine (Xylocaine, Dental adrenalin, 20 mg/ml and 12.5 µg/ml; Astra AB) per hemi-mandible.

Antibiotic prophylaxis was administered using bensylpenicillinprokain-dihydrostreptomycin (25 mg/kg+20 mg/kg, s.i.d, i.m., Streptocillin vet., Boehringer Ingelheim Vetmedica). Animals were intubated and breathing withheld by a ventilator. Vital parameters were monitored continuously (pulse oximetry, rectal temperature, blood pressure, CO_2).

3.5 Tooth extraction

Three contralateral mandibular premolars (P2-P4) and first mandibular molars (M1) were carefully extracted using a minimally invasive surgical approach, i.e., without raising a flap.

3.6 Implant osteotomy and buccal dehiscence defect preparation and implant placement

Implants were placed 20 weeks post-extraction. As depicted in Figure 3, mandibular alveolar ridges were exposed by elevation of a mucoperiosteal flap after midcrestal incision and flattened using a cylindrical cutting bur under saline irrigation. Implant positions for the test and control implants were rotated between left/right and the P3, P4 and M1 positions.

Implant osteotomies were prepared according to the manufacturer's instructions, using the corresponding drills and drill sequences. In brief, osteotomies for group **1** and **2** were prepared as per manufacturer's guidelines for hard bone, using the sequence: Ø2.0 → Ø2.4/2.8 → Ø2.8/3.2 → Tap Drill (Nobel Twist and Step drills, Nobel Biocare AG, Switzerland). Osteotomies for group **3** were prepared as per manufacturer's guidelines for hard bone, using a sequence: Ø2.2 → Ø3.2 → Ø3.5 (only coronal 4 mm) (Velodrill, Institut Straumann AG, Switzerland). Following osteotomy preparation, buccal dehiscence-type defects (3 x 3 x 3 mm) were created with a Lindemann drill as previously described (Figure S2 B) (Schwarz et al. 2008). Briefly, after ridge flattening and osteotomy preparation, a dental probe was used to measure 3 mm in depth from the edge of the ridge. A Lindemann drill (Diameter Ø 0.1 mm; L 9.0 mm, Komet, Germany) was then used to drill perpendicularly into the buccal wall through to the implant osteotomy. This was repeated for the neighboring side of the defect. Then, the edge of the Lindemann was used to cut across, connecting the two drill holes with a through cut. Finally, downward cuts were performed (apical direction) from the ridge down to the original drill holes.

Implants were placed at crestal level using a motorized handpiece followed by a custom-made torque ratchet (Institut Straumann AG, Switzerland). Primary implant stabilities were assessed in terms of maximum insertion torques (max IT).

Implants were subsequently equipped with closure screws and covered by porcine collagen membrane (Geistlich BioGide, Geistlich, Switzerland) followed by primary wound closure (Vicryl® 5.0, Ethicon, USA) for submerged healing. Antibiotic cover and optional analgesia, as described above, were administered for 7 days post-surgery (Streptocilin vet, Boehringer Ingelheim, 3-4 mL/pig i.m.).

3.7 Termination

Animals were sacrificed by intra-cardiac injection of a 20% solution of pentobarbital (Pentobarbitalnatrium, Apoteket AB; Stockholm, Sweden, 60 mg/ml).

Block sections of the implant sites were prepared with an oscillating autopsy saw under perseveration of the soft tissues and fixed in formalin (4 % formaldehyde solution) for at least 2 weeks before histological processing.

3.8 Histological processing

Formalin-treated block sections were dehydrated using ascending grades of alcohol and xylene and, subsequently, infiltrated and embedded in methyl methacrylate (MMA, Sigma Aldrich, USA; Polymerized by Perkadox 16, Nouryon, the Netherlands) for non-decalcified sectioning. Block sections were then cut in a buccolingual direction to sections of 500 µm (EXAKT Systems, Germany)(1 central section per impant) and ground to a final thickness of 30-50 µm. Sections were stained with paragon (toluidin blue and basic fuchsin) for microscopic evaluation.

3.9 Quantitative histomorphometry

Histomorphometric parameters were evaluated on central buccolingual sections of the implant and exclusively on the buccal aspects of the implant (the buccal aspect comprised the defect site). The evaluated histomorphometric parameters are illustrated in Figure S1.

The primary outcome for this study was crestal bone formation. The histomorphometric parameter directly associated with this outcome was:

- New bone height (NBH) as defined by the maximum height of the newly formed bone crest in the defect (Figure S1A)

Secondary outcomes were related to the capacity of the individual implant surfaces to promote osseointegration and bone apposition and included:

- The percentage of bone-to-implant contact in the dehiscence defect area (dBIC) (Figure S1C, ROI 1)
- Vertical bone creep (VBC) as defined by the height of newly formed bone within the defect area in direct contact with the implant (Figure S1D)

- First bone to implant contact (fBIC) as calculated by the distance between the implant shoulder and the most coronal aspect of bone in direct contact to the implant (Figure S1 E).
- Bone area to total area (BATA) as the ratio between the area occupied by newly formed bone and the total defect area (Figure S1B)

Further, the capacity of the implants to promote osseointegration was evaluated by assessing the bone to implant contact in apical native bone (ROI 2) (nBIC) (See Figure S1F).

3.10 Statistical evaluation

Adjusted histomorphometric parameters, 95% confidence intervals (CI), and associations to the different test items under consideration of the factors mandible side and position, in the mandible, were calculated individually for the 2 and 8 week time points using mixed linear regression models (Tables S1 and S2). The adjusted means and the 95% confidence intervals extracted from the models are reported throughout the manuscript.

The correlation between histomorphometric outcomes and the implant geometry, implant surface, and the factors; healing time, mandible side and mandible position were also derived from mixed linear regression models (Table S3). Both models included the factor "animal" as a random effect. The Dunnett-Hsu method was used to adjust for multiple comparisons. The unit of analysis was the subject (animal) and the significance level was set to an alpha <0.05. The software SAS version 9.4 (2016, SAS Institute Inc., Cary, NC, USA) was used for the analysis. The complete set of results from the statistical models are provided as part of supplementary information. The power of the study was calculated post hoc using the obtained parameters at week 8 and setting the level to 0.05 for a two tailed paired test.

4 Results

4.1 Implant geometry comparisons between NGA test implants and geometric replicas and surface characterization

To ensure comparable implant geometries of group **1** and **2,** specifically at the coronal aspect of the implant, interfacing the acute-type dehiscence defect, the three-dimensional implant geometries of both implants were compared by microCT. As evidenced by the 3D overlays in Figure 1B, differences were detected and these were most pronounced in the apical portion of the implants. Specifically, the threads of group **1** were found to be approximately 100 µm

deeper, compared to group **2**, at the apical region. Deviations in the coronal part of the implants were less pronounced, with group **2** showing slightly deeper threads (blue zones in Figure 1C) and a marginally higher coronal platform (orange zones in Figure 1C). The histogram in Figure 1D illustrates that these deviations ranged from -80 to -60 µm in the threads and +60 to +70 µm for the coronal platform height, respectively.

Figure 2 and Table 1 further compares and illustrates the characteristics and parameters related to implant surface topographies, surface roughness and wettability. Scanning electron microscopy (SEM) images and surface roughness measurements of group **1** revealed four zones with changing surface topographies and different Sa values. Specifically, the coronal aspect of group **1** displayed a 2 mm wide zone with a relatively smooth pore-free surface, showing striations and groves and with a relatively low S_a value of 0.662 ± 0.176 µm. Group **1** displayed increasingly pronounced volcano-shaped features, and an associated increase in surface roughness parameters, moving in the apical direction. Specifically, S_a values ranged from 0.680 ± 0.079 µm, at the first transition zone, 3-4 mm from the coronal platform to 1.617±0.208 µm at the implant apex. SEM images of group **2** and **3** revealed a homogenous surface topography displaying micro sized features at two predominant length scales, i.e., periodic pits of diameters between 1–2 µm and 10-50 µm, respectively. The S_a values of group **2** and **3** were 1.206 ± 0.078 µm and 1.315 ± 0.021 µm, respectively. All implants displayed superhydrophilic characteristics with advancing contact angles of 0 ± 0° (Table 1).

4.2 In-vivo investigation

4.2.1 Animal response to implantation and primary stability assessments

All animals recovered from surgery in a predictable manner and without any intra- or post-surgical complications. One of the animals sacrificed at the 2 weeks time point displayed an osteoporotic phenotype as identified during histological processing, characterized by a very thin amount of crestal mandibular bone and a correspondingly large medullary cavity. The resultant histometric measurements were found to be outliers and were thus excluded from the analysis, resulting in 6 and 8 implants per test group for the 2 and 8 week time points, respectively.

All implants displayed appropriate and comparable primary stability as evidenced by insertion torque value measurements for individual time points or averaged over both time points (**1:** 48.3 ± 24.7 Ncm, **2**: 38.0 ± 26.1 Ncm, and **3**: 35.1 ± 24.8 Nm).

Figure 4 compares the histological cross-sections focusing on the buccal dehiscence defects between study groups, after 2 and 8 weeks of healing. All implants healed well and

osseointegrated without any signs of fibrous encapsulation. Healing after 2 weeks was characterized by the formation of a provisional matrix and trabecular primary woven bone that formed starting from the apical margin of the defect. After 8 weeks, the dehiscence defects showed an advanced healing stage, characterized by mature lamellar bone and a widely healed bone crest around all implants. Qualitative differences regarding crestal height and quantity were apparent, with group **2** and **3** displaying a similar increased crestal height and amount of newly-formed bone compared to group **1**. These surface type-associated differences were further analyzed by histology, comparing the detailed healing patterns for group **1** and **2** at higher magnification.

As evidenced by the histological micrographs in Figure 5, distinct qualitative differences in the buccal dehiscence defect healing patterns, around group **1** and **2,** were identified at both healing time points. Specifically, after 2 weeks, differences were related to the degree of mineralization of newly formed bone and the quantity of direct bone apposition to the implant surface (Figure 5A). At the 8 week time point, differences were mainly related to direct bone apposition and the newly formed bone crest (Figure 5B).

After 2 weeks, the healing for group **1** was characterized by new trabecular bone of relatively low mineralization. Interestingly, direct contacts between the newly formed bone matrix and the implant surface were widely absent. By contrast, group **2** showed pronounced bone apposition of newly formed bone in direct contact with the implant surface. Also, the newly formed bone, seen for group **2,** appeared distinctly more mature when compared to group **1,** as based on the ratio between mineralized, frank bone matrix and osteoid, being higher for group 2 than for group 1.

After 8 weeks of healing, the morphology of crestal bone associated with group **1** displayed a wedge-shaped defect-like morphology around the implant surface. This defect-like morphology transitioned into a detectable slit-like gap between the newly formed bone and the implant surface, in an apical direction. Group **2,** by contrast, displayed a horizontal bone crest with mature lamellar bone in direct contact with the implant surface and ongoing crestal osteoid formation at the implant surface.

4.2.2 Histomorphometry

The height and amount of newly formed crestal bone in the dehiscence defect, as a function of group, were histomorphometrically compared after 2 and 8 weeks of healing in terms of NBH and BATA. VBC, fBIC, and dBIC were further assessed to interpret crestal bone formation in

the context of bone apposition to the implant surface and implant osseointegration. Additionally, the groups were compared in terms of implant osseointegration in native apical bone (nBIC). Differences between the 2 and 8 weeks time points were consistent but more pronounced at the 8 weeks time point.

Crestal bone height after 8 weeks, as assessed by NBH, was observed to be significantly higher for group **3** implants (mean 2116µm, 95% CI:1638–2595µm) when compared to group **1** implants (mean 1683µm, 95% CI:1204-2162µm) (p=0.0225). The amount of newly formed crestal bone as evaluated in terms of BATA after 8 weeks of healing was also highest for group **3** (mean 74.30%, 95% CI:65.69–82.82%) and group **2** (66.80%, 95% CI:58.18–75.42%), compared to group **1** (mean 55.45%, 95% CI:46.83–64.07%). Both differences reached statistical significance (p=0.0029 and p=0.0492, respectively) (Figures 6A and B).

Bone apposition and osseointegration as assessed in terms of dBIC (Fig. 6C), VBC (Fig. 6D), and fBIC (Fig. 6E) at the 8 weeks time point were consistently and significantly higher for group **2** and **3,** compared to group **1**. Specifically, group **2** (mean 35.95%, 95% CI:26.36–45.54%) and group **3** (mean 34.90%, 95% CI:25.30–44.49%) showed significantly higher osseointegration in terms of dBIC, compared to group **1** (mean 7.22%, 95% CI:-2.37–16.81%) (p=0.0005 and p=0.0007 respectively). Also, after 8 weeks, group **2** and **3** showed significantly higher crestal bone formation at the implant surface in terms of VBC, i.e., **2** (mean 1519µm, 95% CI:1043-1995µm) and **3 (**mean 1500µm, 95% CI:1025–1976 µm), compared to group **1** (mean 803µm, 95% CI:328–1279µm) (p=0.0029 and p=0.0038, respectively). First bone to implant contact (fBIC) for group **2** and **3** was also significantly higher, when compared to group **1**, i.e. **3** (mean -719µm, 95% CI:-1126– -312µm) and 2 (mean -716µm, 95% CI:-1122– -308µm), compared to group **1** (mean -1772µm, 95% CI:-2179– -1365µm) (p=0.0005 and p=0.0004, respectively).

The osseointegration for group **2** and **3,** in native bone (nBIC) (Fig. 6F), was again significantly higher after 8 weeks of healing compared to group **1**, i.e., **2** (mean 64.92%, 95% CI:51.13–78.71%) and **3** (mean 76.46%, 95% CI:62.69–90.25%), compared to **1** (mean 31.57%, 95% CI:17.79–45.36%) (p=0.0048 and p=0.0007, respectively). Interestingly, nBIC after 2 weeks was significantly higher for group **3** when compared to group **1** (p=0.0011) and **2** (p=0.0083). It may be emphasized that nBIC after 2 weeks was the only parameter and timepoint that showed a strong and significant influence of implant geometry, when comparing group **2** and **3**.

The power of the study to test the null hypothesis of no difference in NBH between implants 1 and 2 (different surfaces and same geometry) was calculated post hoc. The mean study difference between implant 2 and 1 of -263. 02 ± 220.16 mm in NBH (table S2) was used and the alpha level was set to 0.05 for a two tailed paired test. With 8 pairs (subjects) the power of the study is 0.825.

4.3 Influence of study variables on crestal bone formation, osseointegration and bone apposition

A mixed linear regression model was further used to analyze the influence of surface modification and implant geometry on crestal bone formation and osseointegration (Figure S2, Table S6). This model indicated that the surface type significantly affected all histological parameters related to crestal bone formation and osseointegration, except for NBH. Specifically, the model resulted in consistently higher adjusted BATA, dBIC, VBC, and fBIC values for moderately rough implants compared to NGA implants. Interestingly, the bone to implant contact in native bone (nBIC) was the only parameter affected by both implant geometry and surface type, resulting in higher values for the implant geometry of group **3**, compared to the implant geometries of group **1** and **2**. NBH revealed no clear association to either geometry or surface type. All histomorphometric parameters increased with healing time, a majority of which were significant.

5 Discussion

This study investigated the influence of implant surface properties and implant geometry on crestal bone formation in acute-type dehiscence defects and on the osseointegration in native bone. The impact of implant surface properties was examined for two superhydrophilic surface types, i.e., the novel gradient anodized surfaces (NGA, group **1**) and the large-grit sandblasted and acid-etched surface (Moderately rough, group **2**), having the same implant geometry. Additionally, the impact of implant geometry was evaluated using a second tapered implant geometry, also with the moderately rough surface (Group **3**).

From the comparison of the different study groups, the following main observations were obtained: (A) Although NBH was found to be greater for group 1 after 2 and 8 weeks, these differences were not statistically different. Likewise, there were no statistical differences in NBH between groups 2 and 3. The only statistical difference was observed at 12 weeks between groups 1 and 3, with a bigger NBH for group 3. We conclude that the surface properties alone cannot fully account for the differences seen in NBH. (B) all remaining defect-related variables

(BATA, dBIC, VBC and fBIC) were superior for implant groups 2 and 3 at 8 weeks of healing and thus differences may be associated to surface properties (C) Osseointegration in native bone (nBIC) was found to be associated with implant surface properties and the implant geometry. The effect of implant geometry was statistically significant (**1** vs. **3**) at the 2 weeks time point. At the 8 weeks time point, the surface characteristics were found to have the largest impact on nBIC, as no significant difference was observed between group **2** and **3**, while both groups showed significant higher values compared to group **1**.

The influence of implant characteristics on osseointegration has been thoroughly investigated in previous studies. Modification of surface properties, i.e., roughness, wettability and surface energy, implant material or implant geometry have all been shown to strongly influence the process of osseointegration (Rupp et al. 2006; Ogle 2015; Smeets et al. 2016; Wilson et al. 2016). The implant geometries, utilized for the current study, was selected so that group **1** and **2** had the same geometry. Group **3** had a different geometry but was also functionalized with the moderately rough surface, as was the case for group **2**.

Considering that group **2** was a replica of group **1**, some degree of variation is to be expected. The comparison of the implants from group **1** and **2** showed minor deviations and these were mainly localized to the bottom region of the implant threads. Specifically, the threaded region at the coronal part of the implant showed slightly deeper threads, compared to the original. At the apical part, the threads of the replica was found to be more shallow, compared to the reference. Keeping in mind the dimensional scale at which the histomorphometric parameters were assessed, and the magnitude of the variations between groups, for the assessed parameters the potential impact of the dimensional differences between groups **1** and **2** are considered marginal and, therefore, to have a negligible impact on the study outcome.

Since group **2** and **3** showed similar performances, for BATA, dBIC, VBC and fBIC, the results strongly indicate that the superior crestal bone formation observed for group **2** and **3,** compared to group **1,** predominantly arises from differences in surface structures and/or chemistry and are less influenced by the different geometry represented by group **3**.

Schwarz et al. have previously compared the de novo crestal bone formation around titanium implants as a function of surface hydrophilicity in a standardized canine buccal dehiscence type model (Schwarz et al. 2007, 2008). Here, the authors found that crestal bone formation around hydrophilic SLAactive surfaces was enhanced, compared to hydrophobic SLA surfaces (Schwarz et al. 2007). Immunohistological follow-up studies revealed that this enhanced bone formation was associated with the particular ability of the SLActive surface to stabilize the

blood clot, which was essential for the subsequent formation of a well-organized preliminary collagen-rich matrix. On the other hand, less hydrophilic surfaces led to a collapse of the blood clot at the implant surface, which impeded bone formation. Considering that all test groups of the current study show superhydrophilic surface characteristics, the observed differences cannot be contributed to the mechanisms described by Schwarz et al. and, thus, must be contributed to either surface structure or chemistry.

The design of the acute-type dehiscence defect model infers that the surface strucutes presented by the gradient design of group **1** will change as a function of the distance from the coronal aspect, going from relatively smooth towards moderately rough at the apical region. For the current model, the relatively smooth neck of the implant will be exposed in the defect as compared to the moderately rough surface of group **2** and **3**, where the roughness parameters remains the same, along the length of the implant. As a result, the work by Di Iori et al., where the extent of fibrin clot extension as a function of surface roughness was investigated could potentially hint towards the mechanism behind the observations of the current study, relating to the defect site. The authors reported that rough implant surfaces, compared to smooth machined implant surfaces, displayed a significantly increased tendency to promote a more extensive and three-dimensional complex blood clot (Di Iorio et al. 2005). Based on these previous reports, we might hypothesize that differences in crestal bone formation between the moderately rough and NGA surfaces, observed herein, may have been associated with similar effects and differences in the ability of the surfaces to promote blood clot adhesion. The potential importance of implant surface roughness for crestal bone formation might also be indicated by the observation that group **1** implants lacked bone apposition, to the coronal aspect, at the early healing time point. This resulted in the formation of wedge-shaped to slit-like defects between the bone and the implant surface, at the late healing time point. Further, the apical position of the smooth to moderately rough transition of NGA implants (2 mm subcoronal) appear to match with the crestal level of newly formed bone after 8 weeks of healing, indicating that bone formation around NGA implants was limited towards the coronal direction by the presence of the smooth zone at the coronal implant aspect. This is further supported by the study of Botticelli et al. examining the healing of marginal defects, around turned and SLA modified dental implants, in a canine model (Botticelli et al. 2005). Here, inferior defect healing and BIC% was observed for the turned implants.

Analyzing the results of the current study in the light of the findings by Di Iorio et al., Botticelli et al. and those of Schwarz et al., it appears that the effects of superhydrophilicity are not sufficient to ensure optimal osseointegration in the absence of roughness. However, considering

the results for nBIC, roughness alone does not appear to be the sole factor at play. This is the case since inferior performance of group **1** is also observed for the nBIC parameter, measured from the middle to the apical aspect of the implant. Here the roughness of the NGA surface is found to range from S_a 1.079 ± 0.240 (middle) to 1.617 ± 0.208 (apex) µm, compared to the uniform roughness of S_a 1.206 ± 0.078 µm for the moderately rough surface of group **2**. Hence, both surfaces predominantly present moderately rough surface features for ROI 2. Looking at the SEM images presented in Figure 3, it is evident that a comparison of the two surfaces by means of a single roughness parameter is not sufficient. The work by Wennerberg and Albrektsson summarizes the complexity of surface roughness of dental implants and, further, sheds light on this by also addressing the roughness at the nanometer range (Wennerberg & Albrektsson 2009, 2010). Such, in depth, characterization of the different groups has been outside the scope of the current work, however, it would be interesting to further examine the aspects of surface structures and chemistry that might contribute to understanding the current findings.

Concerning the applied animal model, Schwarz et al. reported that acute-type crestal defects displayed a certain tendency to spontaneously heal by bone formation originating from open marrow spaces at the lateral aspects of the defect (Schwarz et al. 2008). A similar self-healing effect might be observed in the porcine model used for the current study as, despite consistently higher histomorphometric parameters related to bone apposition and osseointegration around moderately rough surfaces, the model failed to clearly show differences in new bone height between group **2** and **1**. This aspect may be considered a potential limitation of the applied model when evaluating the results related to new crestal bone height.

Besides crestal bone formation, this study also investigated osseointegration in native bone as a function of implant geometry and surface modifications. Interestingly, implant geometry type B (group **3**) displayed superior osseointegration at the 2 weeks time point, while the geometry type A (group **1** and **2)** was only capable of achieving comparable levels of nBIC, at the 8 weeks time point, when modified with the moderately rough surface. These results illustrate the importance of surface properties to promote osseointegration. They also illustrate that both implant surface and geometry impact synergistically the osseointegration process. Another potential contribution to the observed difference at the 2 weeks time point could be the fact that different implant geometries implies differences in osteotomy preparation. Even though insertion torque values and, thus, the indirect primary stability of the test groups was comparable, a potential positive effect of a shorter drill protocols on the osseointegration for group **3** might not be entirely excluded (Heuzeroth et al.).

As noted above, both investigated technolologies displayed superhydrophilic properties, however, these properties were maintained by two different routes. The superhydrophilic properties of the moderately rough surfaces are maintained by wet-storage (group **2** and **3**) while the NGA (group **1**) surface is maintained by a protective salt layer (Rupp et al. 2006; Lüers et al. 2016; Milleret et al. 2019). The differences in storage condition also represents a difference in the surface chemistry, hence, this might be a factor contributing to the observed differences. Finally, minor differences between the tested implants were related to the implant material (cpTi vs. TiZr). Previous studies failed to show a significant difference in osseointegration between these material types (Saulacic et al. 2012; Gottlow et al. 2012). The effects observed in the current study may, therefore, not be related to the differences in implant materials.

Finally, certain limitations associated with this study should be noted. Overall, these results were obtained within an animal model. Although the semi-quantitative, biological comparisons related to osseointegration are ideally suited to animal setting, the present study does not attempt to claim any aspects are translational in nature. In terms of groups, in order to more clearly separate the influences of the surface and the geometry, a BLX implant with the NGA surface would have needed to be included as a fourth group. Due to the logistical limitation with producing such a group, any conclusions on the implant geometry must remain suggestive in nature. Finally, the defects were created in as standardized a manner as possible. Anatomical differences between animals results in differing buccal thicknesses and thus more or less injured bone to contribute to the regenerative process. However, this was somehow mitigated by allocating groups equally across anatomical positions and by performing the study with a statistically acceptable number of animals. The statistical power of the current study was determined post hoc based on previous experience with similar studies performed using the present animal model.

6 Conclusion

The extent of de novo crestal bone formation in acute-type dehiscence defects appears to be primarily influenced by implant surface characteristics and was in line with the ability of the individual implant surface to promote osseointegration and direct bone apposition.

The potential of the apical, endosteal implant aspects to osseointegrate was influenced by a combination of surface properties and geometry. At early healing time points, implant geometry

modifications can significantly affect endosteal osseointegration and may outperform the effect of surface modifications.

7 References

Albrektsson, T., Zarb, G., Worthington, P. & Eriksson, A.R. (1986) The long-term efficacy of currently used dental implants: a review and proposed criteria of success. *The International Journal of Oral & Maxillofacial Implants* **1**: 11–25.

Atsuta, I., Ayukawa, Y., Kondo, R., Oshiro, W., Matsuura, Y., Furuhashi, A., Tsukiyama, Y. & Koyano, K. (2016) Soft tissue sealing around dental implants based on histological interpretation. *Journal of Prosthodontic Research* **60**: 3–11.

Bosshardt, D.D., Chappuis, V. & Buser, D. (2017) Osseointegration of titanium, titanium alloy and zirconia dental implants: current knowledge and open questions. *Periodontology 2000* **73**: 22–40.

Botticelli, D., Berglundh, T., Persson, L.G. & Lindhe, J. (2005) Bone regeneration at implants with turned or rough surfaces in self-contained defects. An experimental study in the dog. *Journal of Clinical Periodontology* **32**: 448–455.

Buser, D., Chappuis, V., Belser, U.C. & Chen, S. (2017) Implant placement post extraction in esthetic single tooth sites: when immediate, when early, when late? *Periodontology 2000* **73**: 84–102.

Choquet, V., Hermans, M., Adriaenssens, P., Daelemans, P., Tarnow, D.P. & Malevez, C. (2001) Clinical and Radiographic Evaluation of the Papilla Level Adjacent to Single-Tooth Dental Implants. A Retrospective Study in the Maxillary Anterior Region. *Journal of Periodontology* **72**: 1364–1371.

De Bruyn, H., Christiaens, V., Doornewaard, R., Jacobsson, M., Cosyn, J., Jacquet, W. & Vervaeke, S. (2017) Implant surface roughness and patient factors on long-term peri-implant bone loss. *Periodontology 2000* **73**: 218–227.

Di Iorio, D., Traini, T., Degidi, M., Caputi, S., Neugebauer, J. & Piattelli, A. (2005) Quantitative evaluation of the fibrin clot extension on different implant surfaces: Anin vitro study. *Journal of Biomedical Materials Research Part B: Applied Biomaterials* **74B**: 636–642.

Hämmerle, C.H., Brägger, U., Bürgin, W. & Lang, N.P. (1996) The effect of subcrestal placement of the polished surface of ITI implants on marginal soft and hard tissues. *Clinical Oral Implants Research* **7**: 111–119.

Hartman, G.A. & Cochran, D.L. (2004) Initial Implant Position Determines the Magnitude of Crestal Bone Remodeling. *Journal of Periodontology* **75**: 572–577.

Hermann, J.S., Jones, A.A., Bakaeen, L.G., Buser, D., Schoolfield, J.D. & Cochran, D.L. (2011) Influence of a Machined Collar on Crestal Bone Changes Around Titanium Implants: A Histometric Study in the Canine Mandible. *Journal of Periodontology* **82**: 1329–1338.

Huang, X., Bai, J., Liu, X., Meng, Z., Shang, Y., Jiao, T., Chen, G. & Deng, J. (2021) Scientometric Analysis of Dental Implant Research over the Past 10 Years and Future Research Trends. *BioMed Research International* **2021**: 1–13.

Javed, F., Ahmed, H.B., Crespi, R. & Romanos, G.E. (2013) Role of primary stability for successful osseointegration of dental implants: Factors of influence and evaluation. *Interventional Medicine and Applied Science* **5**: 162–167.

Kan, J.Y.K., Roe, P., Rungcharassaeng, K., Patel, R.D., Waki, T., Lozada, J.L. & Zimmerman, G. (2011) Classification of Sagittal Root Position in Relation to the Anterior Maxillary

Osseous Housing for Immediate Implant Placement: A Cone Beam Computed Tomography Study. 5.

Laurell, L. & Lundgren, D. (2011) Marginal Bone Level Changes at Dental Implants after 5 Years in Function: A Meta-Analysis: Marginal Bone Level Changes at Dental Implants. *Clinical Implant Dentistry and Related Research* **13**: 19–28.

Lüers, S., Laub, M. & Jennissen, H.P. (2016) Protecting ultra- and hyperhydrophilic implant surfaces in dry state from loss of wettability. *Current Directions in Biomedical Engineering* **2**: 557–560.

Milleret, V., Lienemann, P.S., Gasser, A., Bauer, S., Ehrbar, M. & Wennerberg, A. (2019) Rational design and in vitro characterization of novel dental implant and abutment surfaces for balancing clinical and biological needs. *Clinical Implant Dentistry and Related Research* **21**: 15–24.

Misch, C.E., Perel, M.L., Wang, H.-L., Sammartino, G., Galindo-Moreno, P., Trisi, P., Steigmann, M., Rebaudi, A., Palti, A., Pikos, M.A., Schwartz-Arad, D., Choukroun, J., Gutierrez-Perez, J.-L., Marenzi, G. & Valavanis, D.K. (2008) Implant Success, Survival, and Failure: The International Congress of Oral Implantologists (ICOI) Pisa Consensus Conference. *Implant Dentistry* **17**: 5–15.

Ogle, O.E. (2015) Implant Surface Material, Design, and Osseointegration. *Dental Clinics of North America* **59**: 505–520.

Percie du Sert N, Hurst V, Ahluwalia A, Alam S, Avey MT, Baker M, et al. (2020) The ARRIVE guidelines 2.0: Updated guidelines for reporting animal research. *PLoS Biol* **18**(7): e3000410.

Pippenger, B.E., Rottmar, M., Kopf, B.S., Stübinger, S., Dalla Torre, F.H., Berner, S. & Maniura-Weber, K. (2019) Surface modification of ultrafine-grained titanium: Influence on mechanical properties, cytocompatibility, and osseointegration potential. *Clinical Oral Implants Research* **30**: 99–110.

Puleo, D. (1999) Understanding and controlling the bone–implant interface. *Biomaterials* **20**: 2311–2321.

Rupp, F., Scheideler, L., Olshanska, N., de Wild, M., Wieland, M. & Geis-Gerstorfer, J. (2006) Enhancing surface free energy and hydrophilicity through chemical modification of microstructured titanium implant surfaces. *Journal of Biomedical Materials Research. Part A* **76**: 323–334.

Schwarz, F., Herten, M., Sager, M., Wieland, M., Dard, M. & Becker, J. (2007) Bone regeneration in dehiscence-type defects at chemically modified (SLActive) and conventional SLA titanium implants: a pilot study in dogs. *Journal of Clinical Periodontology* **34**: 78–86.

Schwarz, F., Rothamel, D., Herten, M., Wüstefeld, M., Sager, M., Ferrari, D. & Becker, J. (2008) Immunohistochemical characterization of guided bone regeneration at a dehiscence-type defect using different barrier membranes: an experimental study in dogs. *Clinical Oral Implants Research* **19**: 402–415.

Smeets, R., Stadlinger, B., Schwarz, F., Beck-Broichsitter, B., Jung, O., Precht, C., Kloss, F., Gröbe, A., Heiland, M. & Ebker, T. (2016) Impact of Dental Implant Surface Modifications on Osseointegration. *BioMed Research International* **2016**: 1–16.

Susin, C., Finger Stadler, A., Musskopf, M.L., Sousa Rabelo, M., Ramos, U.D. & Fiorini, T. (2019) Safety and efficacy of a novel, gradually anodized dental implant surface: A study in Yucatan mini pigs. *Clinical Implant Dentistry and Related Research* **21**: 44–54.

Valles, C., Rodríguez-Ciurana, X., Clementini, M., Baglivo, M., Paniagua, B. & Nart, J. (2018) Influence of subcrestal implant placement compared with equicrestal position on the

peri-implant hard and soft tissues around platform-switched implants: a systematic review and meta-analysis. *Clinical Oral Investigations* **22**: 555–570.
Wennerberg, A. & Albrektsson, T. (2009) Effects of titanium surface topography on bone integration: a systematic review. *Clinical Oral Implants Research* **20**: 172–184.
Wennerberg, A. & Albrektsson, T. (2010) On implant surfaces: a review of current knowledge and opinions. *The International Journal of Oral & Maxillofacial Implants* **25**: 63–74.
Wilson, T.G., Miller, R.J., Trushkowsky, R. & Dard, M. (2016) Tapered Implants in Dentistry: Revitalizing Concepts with Technology: A Review. *Advances in Dental Research* **28**: 4–9.

8 Tables

Table 1: Comparison of surface roughness values and wettability properties of the study implants as stratified by region of interest along the implant long axis. S_a: arithmetic means of the surface points from the mean plane. CA: advancing water contact angle. SD: Standard deviation. N=3.

Implant Group	Property	Coronal Position			
		Collar 1-2 mm	Transition 3 mm	Middle 4-5 mm	Apex 7mm
1	S_a ± SD (µm)	0.662 ± 0.176	0.680 ± 0.079	1.079 ± 0.240	1.617 ± 0.208
	CA	0 ± 0°			
2	S_a ± SD (µm)	1.206 ± 0.078			
	CA	0 ± 0°			
3	S_a ± SD (µm)	1.315 ± 0.021			
	CA	0 ± 0°			

9 Figure Legends

9.1 Figure 1

Figure 1: A) Schematic illustration of study devices: NGA test implants (**1**), moderately rough control implant (**2**), Geometry control implant (**3**). Implants **1** displays NGA surfaces. Implants **2** and **3** are functionalized to show a superhydrophilic, moderately rough, SLA type surface. The geometric shape of implants of group **2** has been replicated from implant of group **1**, i.e., implants **1** and **2** display comparable geometrical shapes (Geometry type A). Implant group **3** displays geometry type B. B) Micro-computer tomography (µCT) image withcolor-coded dimensional variations between NGA test (1) and moderately rough control implants (2)., C) µCT image with colour-coded dimensional variations between the same implants in the coronal region of interest. D) Histogram of dimensional variations. Deviations corresponding to the

peak at 60 – 70 µm were detected primarily at the coronal platform and are related to implant length.

9.2 Figure 2

Figure 2: Overview scanning electron micrograph and zoomed regions of interest (insertions) of implant groups **1** (A; 4 ROIs; coronal ROI with a second ROI insertion at a higher magnification), **2** (B; 1 ROI zoom), and **3** (C; 1 ROI insertion). Bars in main images: 1 mm, bars in insertions: 10 µm, bar in second insertion for the coronal section of the Group 1 implant: 1µm).

9.3 Figure 3

Figure 3: Illustration of individual steps of the surgical procedure. (A) implant osteotomy preparation starting from a flattened mandibular alveolar ridge. (B) & (C) Creation of standardized acute-type buccal dehiscence type defect (3 x 3 x 3 mm). (D) & (E) Implant placement at crestal level (In panel D, the left implant is Group 2; the right implant is Group 3; In panel E, the implant represented is Group 1). (F) Coverage with a collagen membrane. (G) primary wound closure.

9.4 Figure 4

Figure 4: Representative micrographs of histological cross-sections comparing the healing pattern and de-novo crestal bone formation in acute-type dehiscence defects around NGA test implants (1), moderately rough control implants (2), and geometry control implants (3) after 2 weeks (upper row) and 8 weeks of healing (lower row). Insertions show the histological overviews. Scale bar = 1mm.

9.5 Figure 5

Figure 5: Representative histological cross-sections of acute-type dehiscence defects at higher magnification comparing the healing pattern in proximity to NGA and moderately rough implant surfaces of group **1** and **2** after 2 weeks (A) and 8 weeks (B) of healing. (A) 2 weeks of healing: Asterisks denote trabeculae of newly forming bone (osteoid). This early and premature bone type was predominant around implants of group **1**. White arrows indicate early trabecular frank mineralized bone lined by osteoid seams. This more mature bone type appeared dominant around implants of group **2**. The white double arrow marks the length of the implant surface in contact with newly formed bone (from withing the original defect area). Bone apposition to moderately rough surfaces was more pronounced as compared to NGA surfaces.

(B) 8 weeks healing: NGA implant surfaces were characterized by a wedge-like gap at the coronal aspect of the dehiscence defect that transitioned into a thin non-mineralized slit-like gap, interposed between the implant surface and newly formed lamellar bone in the apical direction (white arrow). The small red arrow and double arrow mark the extent of epithelial downgrowth detected at the coronal aspects of the implant surface and the extent of the zone in which this epithelium was apparent, respectively. Moderately rough implant surfaces were characterized by mature lamellar bone in direct contact with the implant surface (white double arrow). Small white arrows mark osteoid at the crestal aspects of newly formed bone. Scale bar = 500µm

9.6 Figure 6

Figure 6: Comparison of histomorphometric parameters between different implant groups after 2 and 8 weeks of healing: A) NBH: new crestal bone height, B) BATA: Ratio of bone area to total area in the defect (ROI 1), C) dBIC: bone to implant contact in the dehiscence defect area (ROI 1) D) VBC: vertical bone creep, E) fBIC: first bone to implant contact, F) nBIC: native bone to implant contact in the apical region of interest (ROI 2). Individual values represent adjusted mean values by mixed linear regression. Error bars designate the 95% confidence intervals. Levels of significance as adjusted according to Dunnet-Hsu: * $p \leq 0.05$, ** $p \leq 0.01$, *** $p \leq 0.001$.

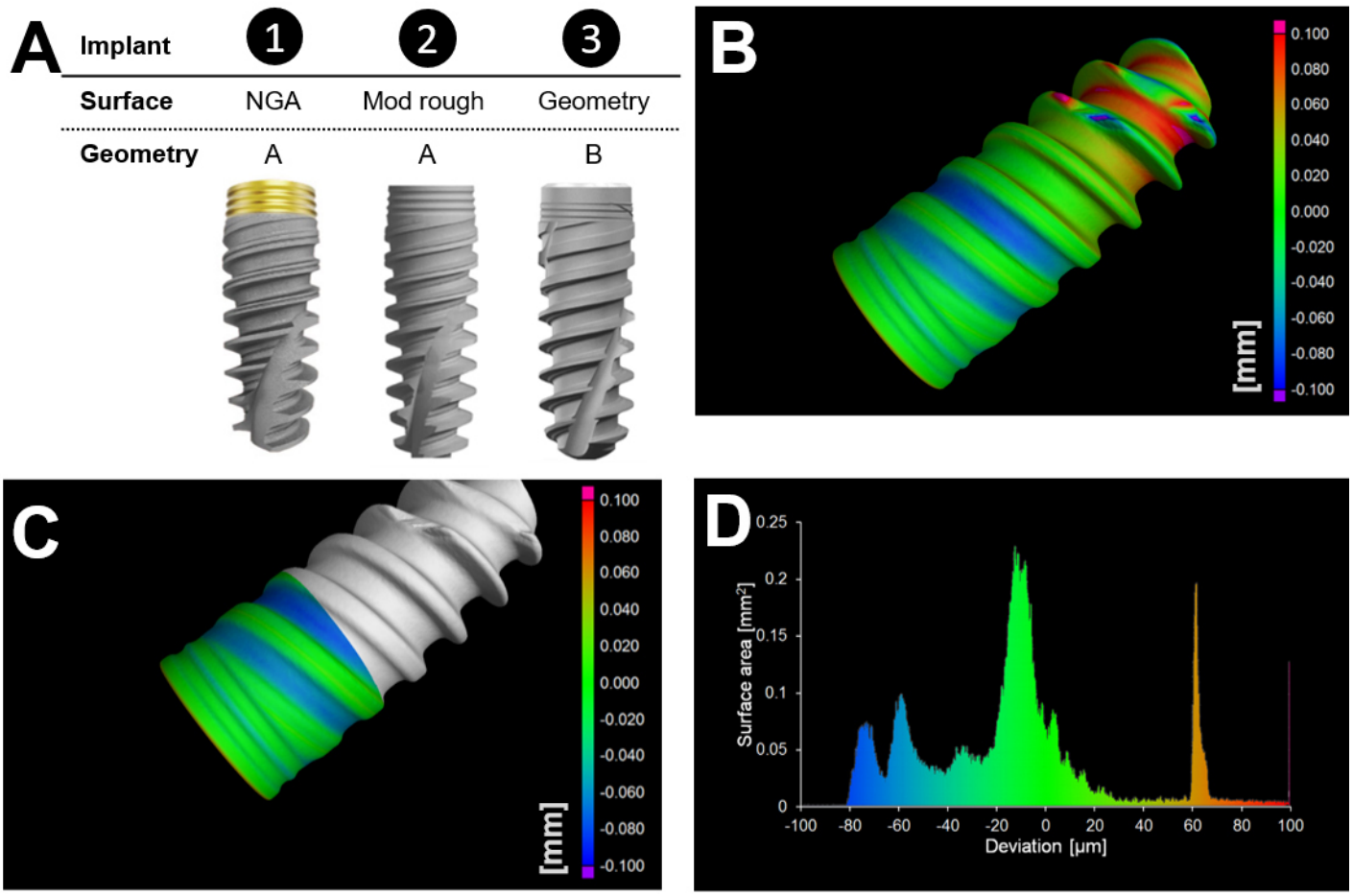

CLR_13996_Figure 1.jpg

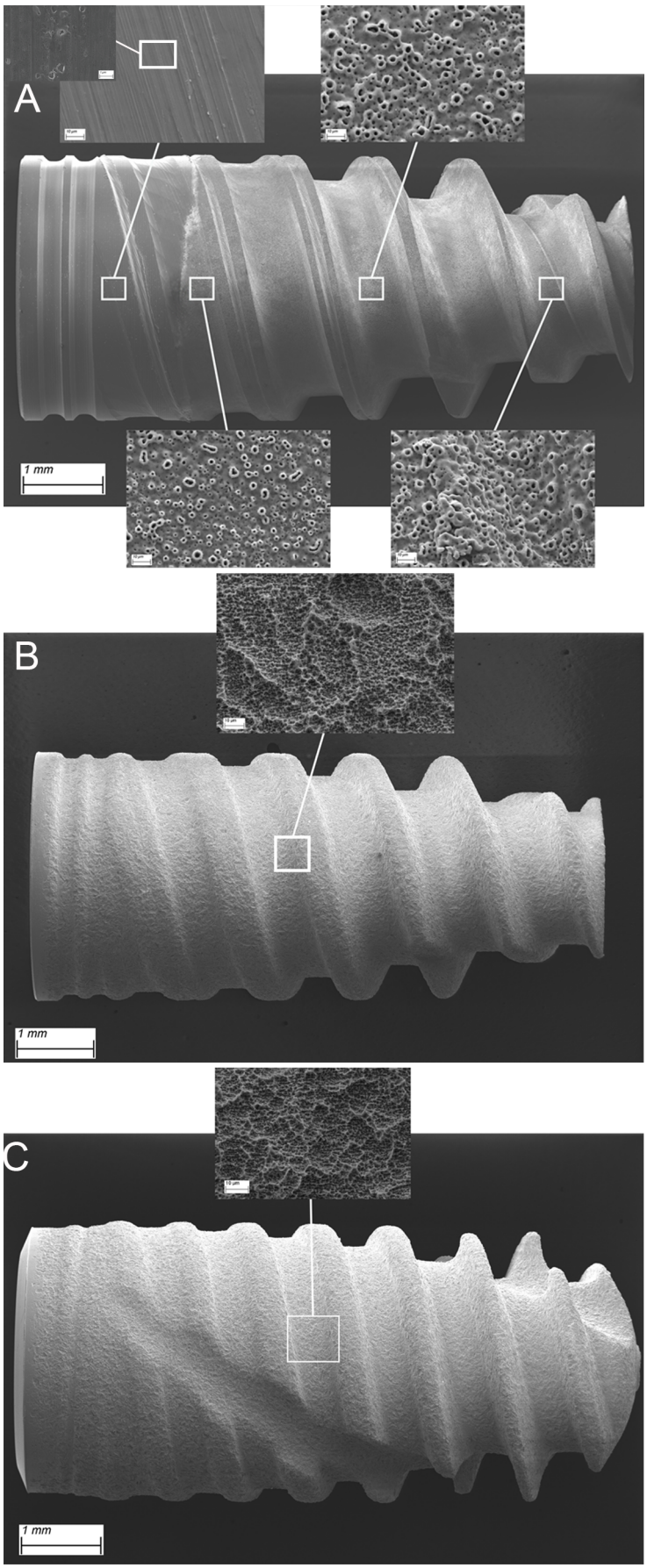

CLR_13996_Figure 2.tif

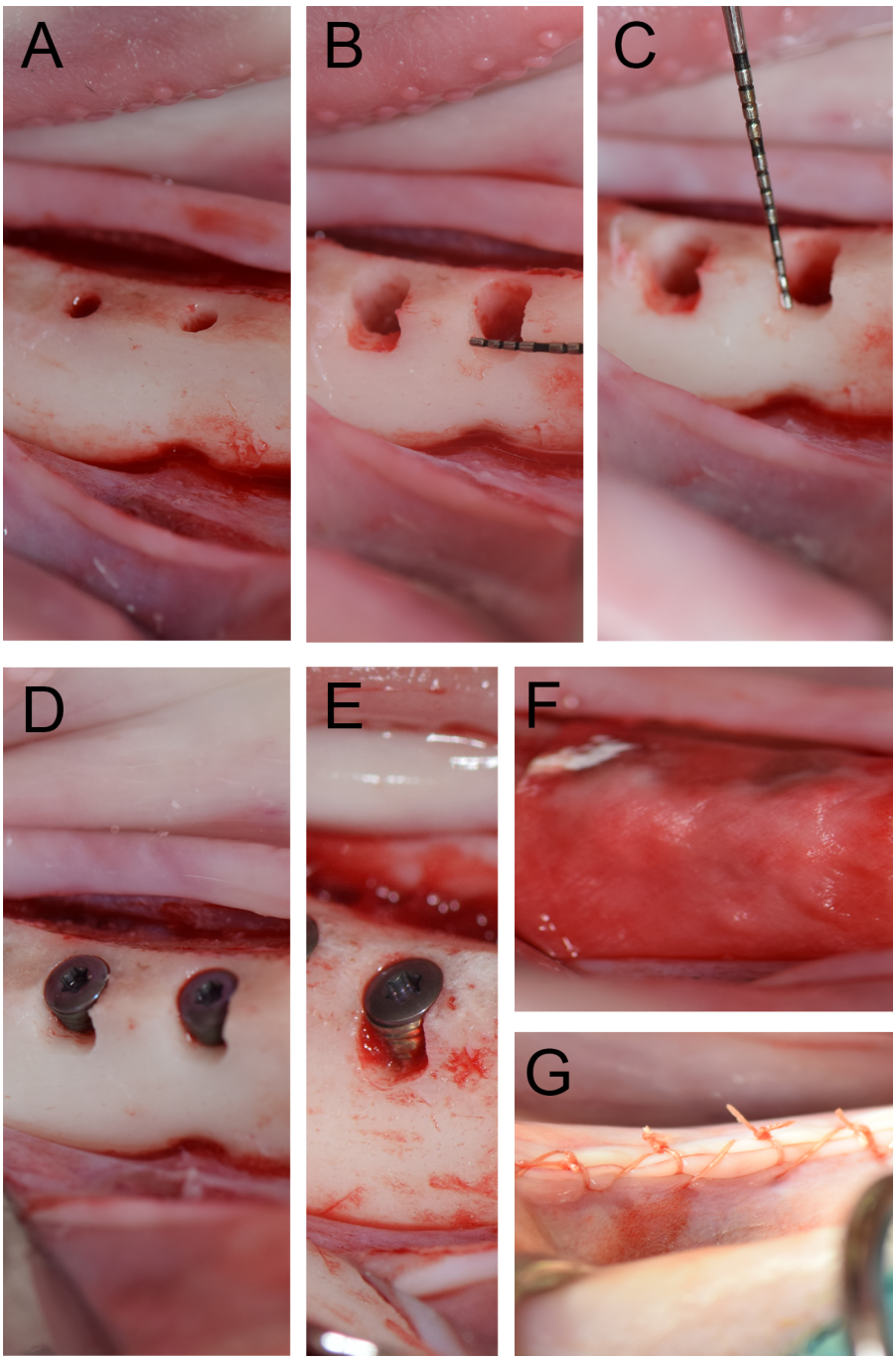

CLR_13996_Figure 3.tif

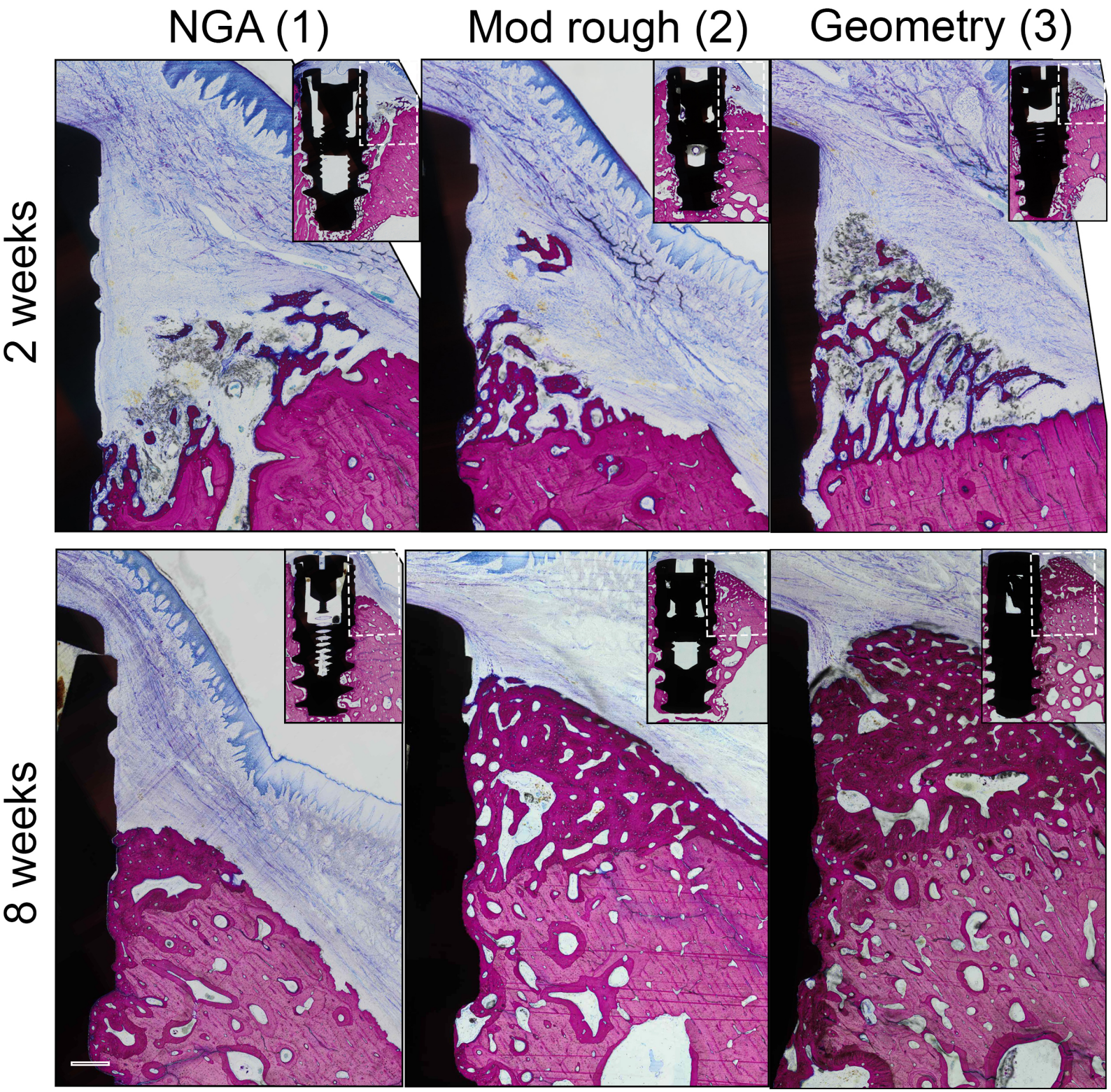

CLR_13996_Figure 4.tif

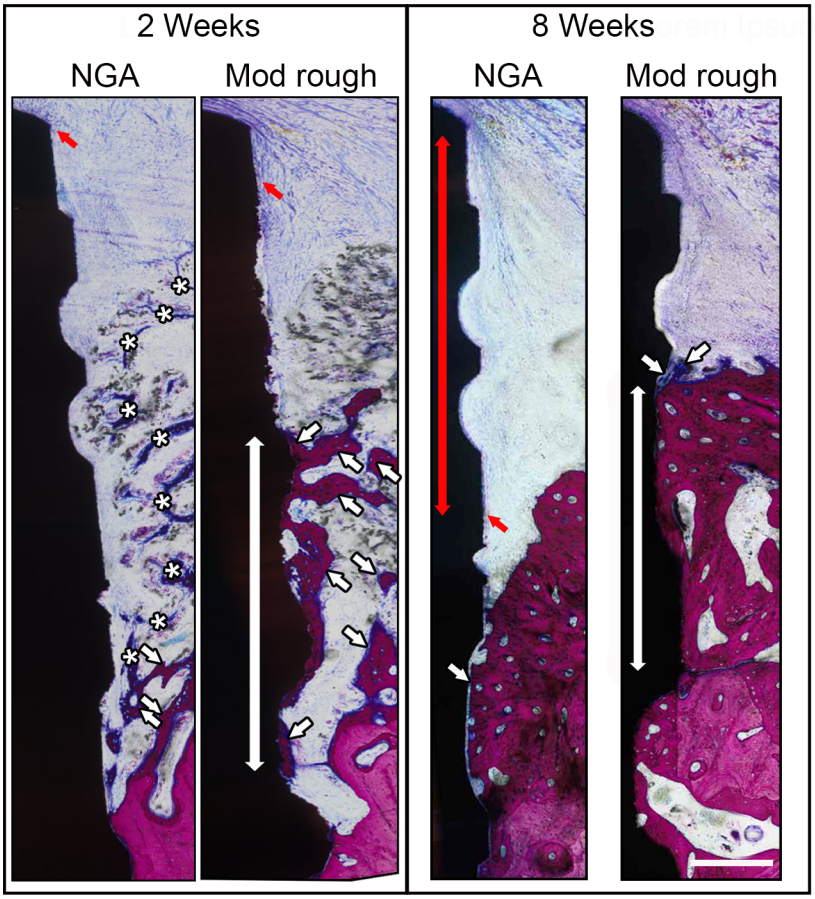

CLR_13996_Figure 5.tif

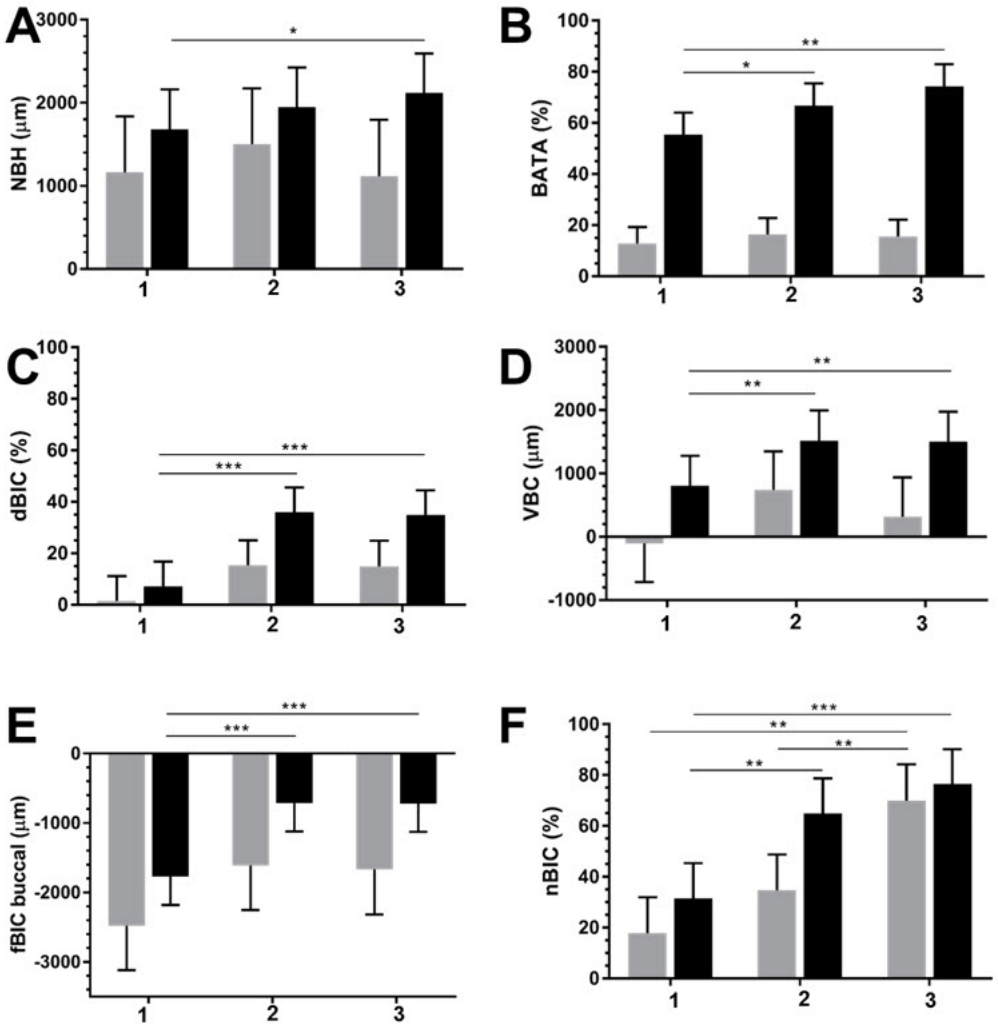

CLR_13996_Figure 6.tif